Research Article | Vol. 26, No. 26 | 24 Dec 2018 | OPTICS EXPRESS A974
Optics EXPRESS

Enhanced photovoltaic performance of nanowire array solar cells with multiple diameters

XIN YAN,[1,4] LEI GONG,[1,4] LINGMEI AI,[1] WEI WEI,[2,3] XIA ZHANG,[1,*] AND XIAOMIN REN[1]

[1]*State Key Laboratory of Information Photonics and Optical Communications, Beijing University of Posts and Telecommunications, Beijing 100876, China*
[2]*School of Mechanical and Electric Engineering, Guangzhou University, Guangzhou 510006, China*
[3]*Photonics Research Centre, Department of Electronic and Information Engineering, The Hong Kong Polytechnic University, Hung Hom, Kowloon, Hong Kong, China*
[4]*These authors contributed equally*
**xzhang@bupt.edu.cn*

Abstract: A multi-diameter p-i-n junction GaAs nanowire (NW) array architecture is proposed for high-performance solar cells. Coupled three-dimensional optoelectronic simulations are performed to investigate the photovoltaic properties. The NW diameters are randomly selected within the range of 220–400 nm, following the Gaussian distribution. The results show that the absorption strongly depends on the diameter, and the multi-diameter NW array exhibits higher optical absorption, in comparison with the uniform-diameter counterpart. This is because of the superposition of multiple absorption peaks. Moreover, the multi-diameter NW array can efficiently enhance the effective absorption; that is, the depletion region absorption, which directly leads to increased photocurrent. A remarkable efficiency of 17% is obtained for a 16-diameter NW array solar cell with a full width at half maximum of the diameter distribution of 75 nm, higher than the best value (16.1%) of uniform-diameter device with an optimum diameter of 310 nm. This work demonstrates that the native diameter nonuniformity of self-organized nanowires is beneficial for high-performance photovoltaics with low cost and a simple fabrication process.

1. Introduction

With the growing energy consumption and deteriorating climate problems, photovoltaic technology has gain increasing attention due to its inexhaustibility, cleanability, and security. Nowadays various new technologies have been developed to achieve low-cost high-efficiency solar cells, including black silicon, plasmonics, diffractive structures, nanocrystals, quantum dots, and nanowires (NWs) [1–6]. Among these technologies, NWs have shown unique potential as they play the role of both the light trapping and concentrating structure and photoelectric converser, enabling small-size, low-cost, and high-integration solar cells [7,8]. In addition, the ultrasmall footprint area of NWs leads to high tolerance of lattice-mismatch, enabling the realization of high efficiency tandem solar cells, or flexible solar cells on cheap substrates [9–11]. The structural parameters of the NW array (NWA) play a critical role in the performance of solar cells as they determine the optical absorption and carrier separation and transportation. So far, many efforts have been made to design the parameters of the NWA, including the morphology, orientation, diameter/periodic (D/P) ratio, diameter, as well as length [12–15].

At present, most of the vertically-aligned NWA solar cells are based on NWs with uniform diameters [16–18]. Both theoretical and experimental results demonstrate that the absorption of NWA strongly depends on the diameter [19–21]. For small diameter NWs, less optical modes are supported, resulting in poor absorption of long wavelength light. For large

#349814 https://doi.org/10.1364/OE.26.00A974
Journal © 2018 Received 1 Nov 2018; revised 14 Dec 2018; accepted 14 Dec 2018; published 19 Dec 2018

Optics EXPRESS

diameter NWs, although the absorption of long wavelength modes is significantly improved, the absorption of short wavelength light is reduced due to the increased reflection at the top surface of the NWA. That is, the absorption peak wavelength strongly depends on the NW diameter. For the NWA with uniform diameter, the absorption is not uniform. Hence, the uniform-diameter NWA is probably not the optimal structure for solar cells, from the perspective of optical absorption.

Due to the selective absorption feature of NWs, NWA with multiple diameters is expected to have high and uniform absorption over a broad wavelength range [22]. In addition, NWAs with uniform diameter typically require complex fabrication processes, such as nanoimprinting lithography and electron beam lithography (EBL), which drastically increase the development time and device cost [16–18]. Conversely, the fabrication process of multi-diameter NWAs is very simple, as the diameter of NWs grown by the popular vapor-liquid-solid (VLS) mechanism is naturally nonuniform and follows the Gaussian distribution [23–25]. Moreover, limited by the EBL process, it's difficult to fabricate a uniform-diameter NWA with large area. However, it's easy to achieve a wafer-scale multi-diameter NWA as the lithography is not required. Hence, NWAs with a Gaussian diameter distribution are potentially superior to uniform-diameter approaches not only in terms of efficiency, but also in terms of simplicity, low-cost, reproducibility and scalability from the point of view of the photovoltaic industry. In this paper, we have proposed a solar cell architecture based on a multi-diameter GaAs NWA. GaAs material is selected due to its optimum bandgap relative to the 1-sun air mass 1.5 global (AM1.5G) spectrum. Up to 16 diameters are adopted to simulate a practical NWA whose diameters follow the Gaussian distribution. Each NW contains an axial p-i-n junction, which is widely used for photoelectric conversion in practical NWA solar cells [10,16,17]. A coupled three-dimensional (3-D) optoelectronic simulation is performed to investigate the optical absorption and photoelectric conversion of the structure in detail. The results show that the multi-diameter NWA has higher optical absorption in comparison with the uniform one due to the superposition of multiple absorption peaks. A remarkable efficiency of 17% is obtained for a 16-diameter NWA, higher than the best value (16.1%) of uniform-diameter device with an optimum diameter.

2. Simulations

Figure 1(a) illustrates the schematic of the uniform-diameter NWA solar cell, which consists of periodic axial p-i-n GaAs NWs on a GaAs substrate. The GaAs substrate is n-doped with the carrier concentration fixed at 1×10^{17} cm^{-3}. In order to save the resources and time required for the calculation, the thickness of the GaAs substrate is limited to 400 nm. However, by using a perfect match layer (PML) adjacent to the substrate, the transmission light is totally absorbed, which enables us to model a semi-infinite substrate. The NWs have a total length of 2 μm, in which both the p- and n-regions have a length of 200 nm and are regularly doped to 3×10^{18} and 1×10^{17} cm^{-3}, respectively [26]. The NW length is comparable to the thickness of a planar solar cell, which is sufficient long for the light absorption [14]. The length of bottom n-region has little influence on the performance, while the length of top p-region should be small enough to reduce the recombination losses. However, for an effective contact with the electrode, the top p-region shouldn't be too short. Hence, a moderate length of 200 nm is selected for both the p and n regions. The D/P ratio determined by the period of the square lattice (P) and the diameter of NWs (D) is fixed at 0.5, which is shown to maximize the absorption in periodic GaAs NWAs [20]. Figures 1(b) and 1(c) show the multi-diameter NWA solar cells with 4 and 16 different diameters, respectively, which have the same structural parameters, i. e. D/P ratio, length, and doping level, except for the diameters. The diameters are randomly selected near the optimal diameter at which the uniform-diameter NWA solar cell has the highest conversion efficiency.

Optics EXPRESS

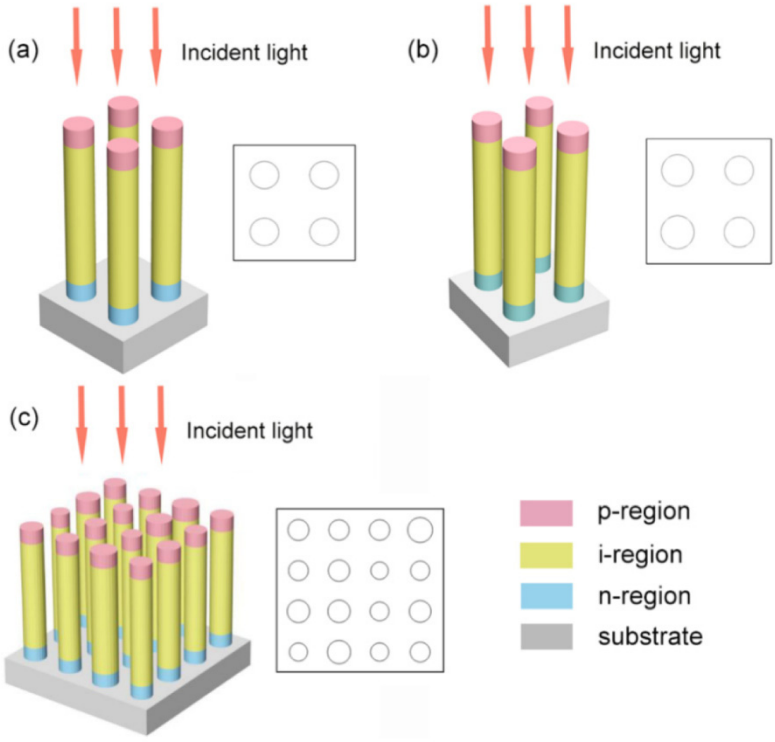

Fig. 1. 3-D schematics and top views of one unit cell of uniform-diameter (a), 4-diameter (b), and 16-diameter (c) NWA solar cells.

The absorption and photovoltaic properties of the devices are investigated through Sentaurus Electromagnetic Wave (EMW) Solver and Sentaurus Device (SDEVICE) module package. The NWA is theoretically analyzed by using 3-D FDTD simulations. The minimum cell size of the FDTD mesh is set to 5 nm, and the number of nodes per wavelength is 20 in all directions. By placing periodic boundary conditions in the x and y directions, the simulations are carried out within a unit cell to model the periodic square-array wire structure. The simulation domain is closed at the top and bottom with a perfectly matched layer, allowing reflected light and transmission light to escape the simulation volume. The wavelength-dependent complex refractive index used in the simulations is obtained from Levinshtein's work [27]. The NWA is illuminated by sunlight from the top, and plane wave defined with power intensity and wavelength values from a discretized AM 1.5G solar spectrum is used to model the sunlight. The AM 1.5G spectrum is divided into 62 discrete wavelength intervals, from 290 to 900 nm (typical absorption region of GaAs). The transverse electric (TE) and transverse magnetic (TM) mode contributions are superimposed to model the corresponding unpolarized feature of sunlight. The total optical generation under AM 1.5G illumination can be modeled by superimposing the power-weighted single wavelength optical generation rates. The optical generation rate G_{ph} is obtained from the Poynting vector P [28]:

$$G_{ph} = \frac{\left|\vec{\nabla}\cdot\vec{P}\right|}{2\hbar\omega} = \frac{\varepsilon''\left|\vec{E}\right|^2}{2\hbar} \quad (1)$$

where E is the electric field intensity at each grid point, ω the angular frequency of the incident light, $\hbar$ is the reduced Planck's constant, and ε'' is the imaginary part of the

Optics EXPRESS

permittivity. The reflection monitor is located at above the top surface of the NWA, while the transmission monitor is located at the bottom surface of substrate to calculate the light absorbed. The amount of power transmitted through the power monitors is normalized to the source power at each wavelength. The reflectance $R(\lambda)$ and transmission $T(\lambda)$ are calculated by the equation:

$$R(\lambda), T(\lambda) = \frac{0.5\int real\{P(\lambda)_{monitor}\}dS}{P_{in}(\lambda)} \tag{2}$$

where $P(\lambda)$ is the Poynting vector, dS is the surface normal, and $P_{in}(\lambda)$ is the incident source power at each wavelength. The absorption spectrum $A(\lambda)$ of the GaAs NWA is given by the following equation

$$A(\lambda) = 1 - R(\lambda) - T(\lambda) \tag{3}$$

For the electrical modeling, the 3-D optical generation profiles are incorporated into the finite-element mesh of the NWs in the electrical tool, which solves the carrier continuity equations coupled with Poisson's equation self-consistently in 3D. In the electrical simulation, the doping-dependent mobility and bandgap narrowing, as well as the radiative, Auger and Shockley-Read-Hall (SRH) recombination, are taken into consideration. The NWs are assumed to be perfectly passivated, which means that the surface recombination velocity (SRV) is in the order of 10^3 cm/s [29–31]. Hence in our simulations, the SRV is neglected for simplicity as previous work has demonstrated that a low SRV of 10^3 cm/s has little influence on the device performance [14]. The critical material parameters for device simulations are mainly obtained from Levinshtein's work [27].

3. Results and discussion

The photovoltaic performance of uniform-diameter NWA solar cells is firstly simulated to find the optimal diameter at which highest conversion efficiency is obtained. Figure 2(a) shows the optical absorption spectra for NWAs with different diameters in the range of 220–400 nm. Obviously, the absorption peak shifts to longer wavelength with the increase of NW diameter. For small diameter NWs, the absorption quickly drops at long wavelengths. While for large diameter NWs, the absorption becomes weak at short wavelengths. Figure 2(b) shows the current density-voltage (J-V) curves of NWA solar cells with different diameters under AM 1.5G illuminations. It can be seen that for different diameter NWA solar cells, the open-circuit voltage (V_{oc}) is almost the same, while the short-circuit current density (J_{sc}) is different. The maximum conversion efficiency is 16.1% at the diameter of 310 nm, corresponding to an optimal total absorption over the whole solar spectrum.

Optics EXPRESS

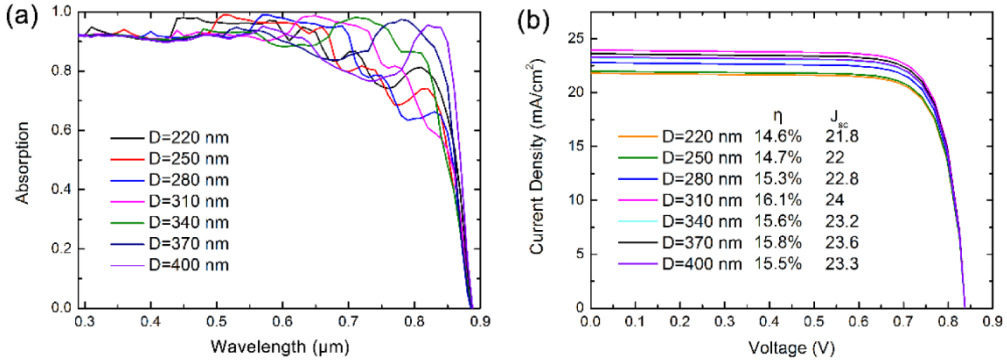

Fig. 2. (a) The dependence of absorption on wavelength for uniform-diameter NWAs with different diameter. (b) The J-V characteristics of uniform-diameter NWAs with different diameter.

Now we turn to study the photovoltaic performance of multi-diameter NWA solar cells. For simplicity, a 4-diameter NWA solar cell is firstly investigated. 4 diameters are randomly selected in the range of 220–400 nm with a center diameter of 310 nm. The centers of the NWs in the 4-diameter NWA coincide with those in the uniform-diameter NWA with a diameter of 310 nm. Figure 3(a) shows the absorption spectra of 5 different NWAs, each of which contains a group of 4 different diameters randomly generated by the computer. It can be seen that the absorption spectra of the 5 NWAs are close to each other with little deviation. Figure 3(b) shows the absorption of a 4-diameter NWA with diameters of 285, 300, 317, and 332 nm. The absorption of a uniform-diameter NWA with diameter of 310 nm is also plotted for comparison. It can be seen that the 4-diameter NWA exhibits higher absorption than the uniform-diameter one in the wavelength range of 710–850 nm. To explain the absorption enhancement in the long wavelength range, the absorption spectra of each diameter NWs is investigated, as shown in Fig. 3(c). It can be seen that the absorption strongly depends on the NW diameter. For example, for 285 nm NWs, the absorption is high in the range of 300–400 and 600–700 nm, but quickly drops after 700 nm. While for 332 nm NWs, the absorption is high in the range of 700–800 nm, but low at short wavelengths. It is clear that each diameter corresponds to a certain absorption peak, which shifts to longer wavelength as the diameter increases. The multi-diameter NWA combines these absorption peaks and exhibits near-flat and high absorption over the whole solar spectrum, as shown in Fig. 3(b). Figure 3(d) shows the J-V characteristics of the 4-diameter and uniform-diameter NWA solar cells. Under AM 1.5G illumination, the 4-diameter device exhibits a V_{oc} of 0.842 V and J_{sc} of 24.7 mA/cm^2, yielding a conversion efficiency of 16.6%, higher than the maximum efficiency (16.1%) of uniform-diameter NWA solar cells.

A practical NWA typically contains a great deal of diameters which obey the Gaussian distribution. In order to simulate a practical NWA, 16 diameters are randomly generated by computer in the range of 220–440 nm, which follow the Gaussian distribution with an expectation of 310 nm. The NWs are squarely arranged with the smallest repeatable unit cell as identified in Fig. 1(c), whose centers coincide with those of the 310 nm NWA. Figure 4 shows the distribution of the 16 diameters [265, 277, 278, 288, 292, 303, 304, 311, 313, 321, 327, 332, 343, 344, 356, 381] nm, which are fitted by a Gaussian curve. The mean diameter, standard deviation, and full width at half maximum (FWHM) are calculated to be 314 nm, 31.6 nm, and 75 nm, respectively. Figure 5(a) shows the absorption spectra of the NWA. The absorption spectra of a uniform-diameter NWA with a diameter of 310 nm and 4-diameter NWA are also plotted for comparison. It can be seen that the 16-diameter NWA exhibits high and near flat absorption over a broad wavelength range of 300–820 nm. In comparison with the uniform-diameter and 4-diameter NWAs, the absorption at long wavelengths is significantly enhanced. Figure 5(b) shows the absorption spectra of each diameter NWs in

Optics EXPRESS

the16-diameter NWA. Similar to the spectra in Fig. 3(c), the absorption of NWs strongly depends on the diameter. According to the absorption peak, the spectra can be divided into several groups, as shown in Figs. 5(c)–5(f). For diameters of 265, 277, and 278 nm, the absorption peaks are in the range of 600–650 nm. For diameters of 288, 292, 303, 304, and 311 nm, the absorption peaks are in the range of 650–700 nm. For diameters of 313, 321, 327, and 332 nm, the absorption peaks are in the range of 700–800 nm. For largest diameters of 343, 344, 356 and 381 nm, the absorption peaks are around 800 nm. The multiple absorption peaks superpose together, resulting in high and flat absorption over a broad wavelength range. According to the spectra in Fig. 5(a), it can be concluded that large diameter NWs, whose absorption peaks are beyond 700 nm, mainly contribute to the absorption enhancement at long wavelengths. Small diameter NWs are also important for the total absorption enhancement, which compensate the absorption drop of large diameter NWs at short wavelengths.

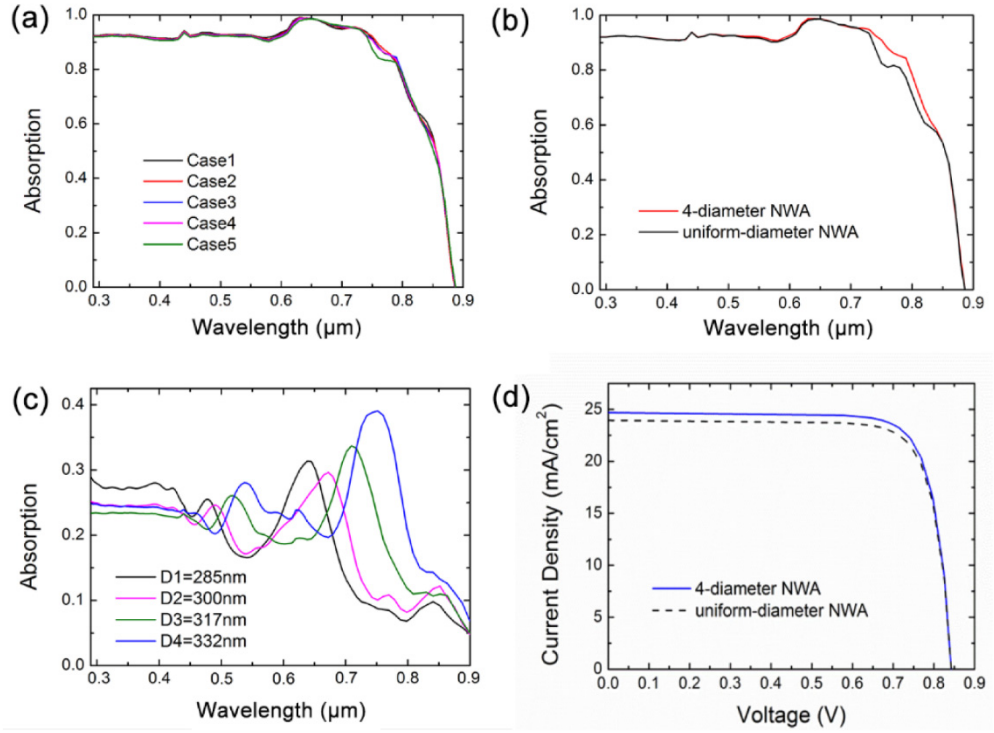

Fig. 3. (a) Absorption of five different 4-diameter NWAs. (b) Absorption vs. wavelength for the uniform-diameter NWA with a diameter of 310 nm and 4-diameter NWA with 4 random diameters (285 nm, 300 nm, 317 nm, 332 nm). (c) Absorption vs. wavelength for each diameter NWs in the 4-diameter NWA. (d) The J-V characteristics of the uniform-diameter and 4-diameter NWA solar cells.

Optics EXPRESS

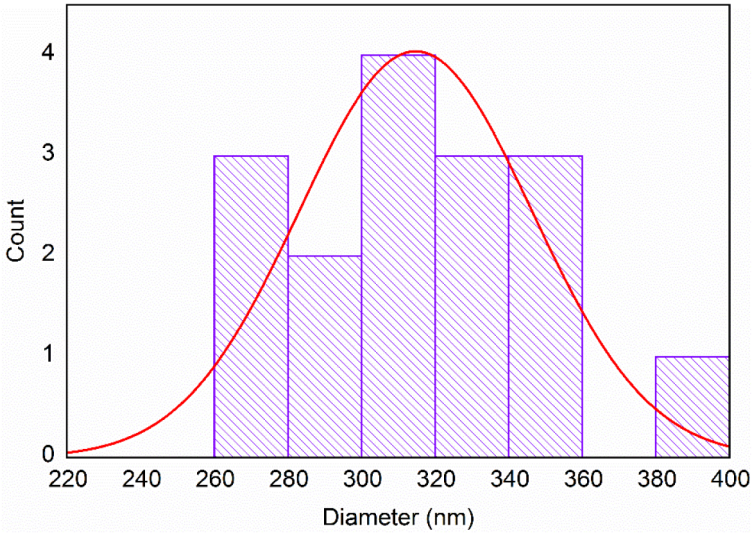

Fig. 4. Statistics of the selected 16 diameters and the fitted Gaussian distribution curve.

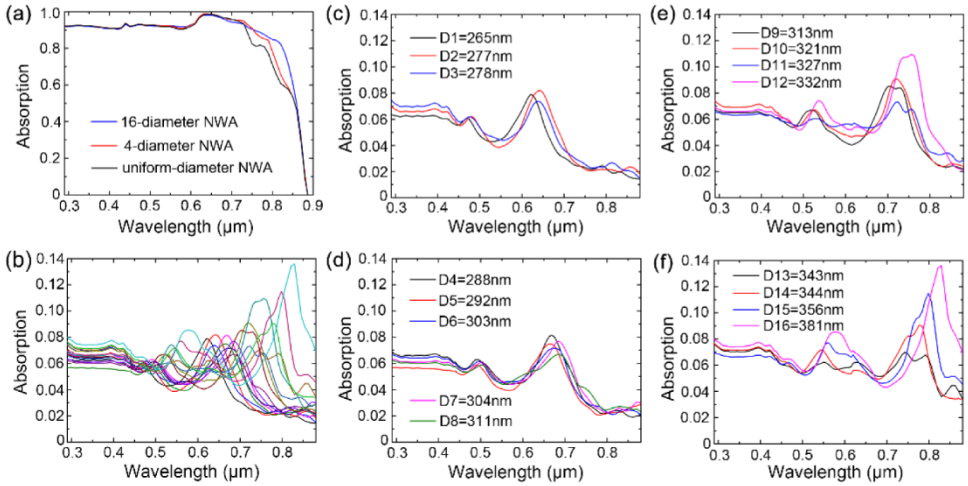

Fig. 5. (a) Absorption spectra of the 16-diameter NWA with 16 random diameters (265, 277, 278, 288, 292, 303, 304, 311, 313, 321, 327, 332, 343, 344, 356, 381) nm, the 4-diameter NWA with 4 random diameters (285, 300, 317, 332) nm, and the uniform-diameter NWA with a diameter of 310 nm. (b) Absorption spectra of each diameter NWs in the 16-diameter NWA. (c) –(f) Absorption spectra of NWs in the 16-diameter NWA with similar absorption peaks.

From Fig. 5(a) it can be seen that the uniform-diameter NWA exhibits two absorption valleys at 760 and 820 nm, which are filled up in the absorption curve of the 16-diameter NWA. Hence the absorption enhancement at the two wavelengths should be the most obvious. Figures 6(a) and 6(b) present the vertical cross sections of optical generation profiles in NWs at wavelength of 760 and 820 nm under TM polarization. At 760 nm, photon generation is mainly concentrated on the top of NWs in the uniform-diameter NWA. As the absorption in the middle depletion region mainly contributes to the photocurrent while the photocarriers generated in the top p region quickly recombine due to lack of built-in electric field, the NWA with uniform diameter of 310 nm has poor photoresponse to the incident 760 nm light [6,13]. For the 16-diameter NWA, the photo generation permeates the entire NWs with a diameter of 321, 313, 327, and 332 nm, leading to strong photoresponse to the incident

Optics EXPRESS

760 nm light. At a longer wavelength of 820 nm, few modes can be confined in the 310 nm NWs, as shown in Fig. 6(b). While in the 16-diameter NWA, large diameter NWs including 343, 344, 356, and 381 nm, can support optical modes and have high absorption across the whole NWs. Hence the multiple diameters not only increase the total absorption at certain wavelengths, but also enhance the effective absorption, that is, the absorption by the depletion region, which will directly lead to the enhancement of conversion efficiency [13].

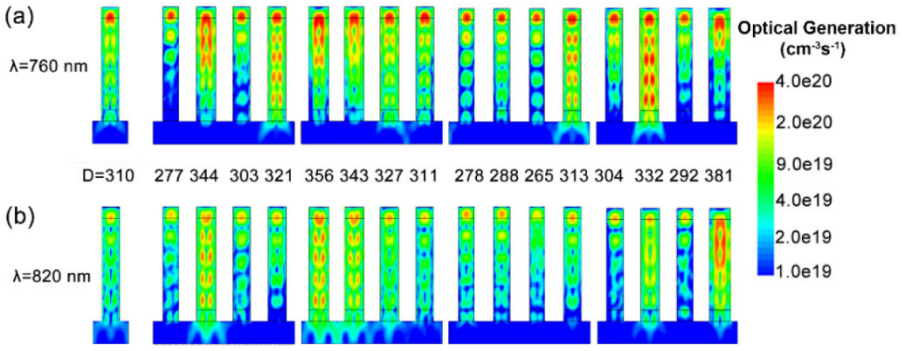

Fig. 6. Vertical cross sections of optical generation profiles of the uniform-diameter NWA with a diameter of 310 nm and the 16-diameter NWA at wavelength of (a) 760 nm and (b) 820 nm.

The simulated photo generation profiles are then incorporated into the electrical tool to calculate the terminal J-V characteristics of 16-diameter NWA solar cells. From Fig. 7 it can be seen that the 16-diameter NWA solar cell yields higher short-circuit current density than the uniform-diameter and 4-diameter counterparts, in accordance with the absorption enhancement presented in Fig. 5(a). The conversion efficiency of the 16-diameter, 4-diameter, and uniform-diameter solar cells is 17%, 16.6%, and 16.1%, respectively. It should be pointed out that no serial resistance losses and no leakage currents were assumed in the analysis. Table 1 lists the main parameters of our best device and other reported GaAs p(i)n junction NWA solar cells. It can be seen that our 16-diameter device exhibits higher efficiency in comparison with other reported uniform-diameter devices.

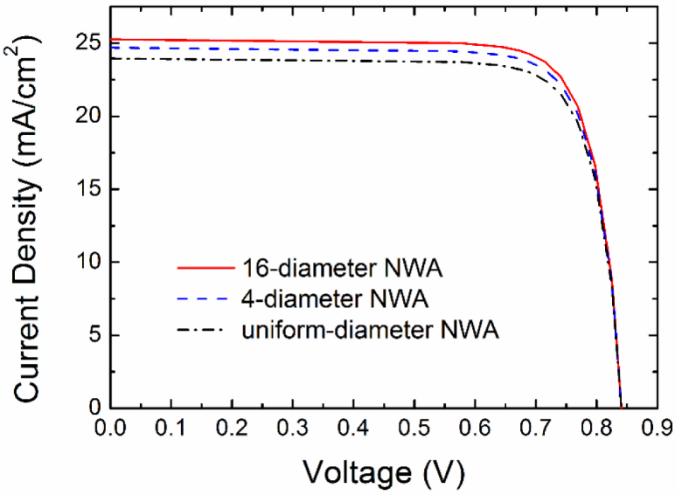

Fig. 7. The J-V characteristics of the 16-diameter, 4-diameter, and uniform-diameter NWA solar cells.

Optics EXPRESS

Table 1. Main parameters of the reported GaAs p(i)n junction NWA solar cells.

Mean diameter (nm)	FWHM (nm)	Effective thickness (nm)[1]	V_{oc} (V)	J_{sc} (mA/cm^2)	Efficiency	Ref.
314	75	400	0.841	24.3	17%	This work
200	–	157	0.888	16.4	11.7%	[14]
215~245	–	370	0.906	21.3	15.3%	[16]
320	–	559	0.565	21.08	7.58%	[17]
290	–	239	0.57	18.9	7.53%	[26]

[1]The effective thickness is the ratio between the volume of NWs and the illuminated surface area [32].

Finally, we give a short description of the realization of the proposed architecture. The fabrication process is similar to the widely reported GaAs NWA solar cells, but simpler [16–18]. Generally speaking, GaAs NWs are grown by a simple VLS method using metal organic chemical vapor deposition (MOCVD) or molecular beam epitaxy (MBE). Multiple diameters following the Gaussian distribution are achieved by controlling the deposition time and annealing temperature of catalyst [25]. For the fabrication of electrodes, NWAs are firstly covered with transparent dielectric, e. g. polyimide by spin casting. The transparent dielectric is then removed from the tips for electrode contact. A transparent conducting oxide (TCO) electrode is then sputtered onto the NWA, followed by heat treatment to reduce the resistance. The back-side is attached with Ag glue to a brass coin, serving as back contact.

4. Conclusion

In summary, we have proposed a multi-diameter GaAs NWA solar cell structure and investigated its optical absorption and photovoltaic properties by using a coupled 3-D optoelectronic simulation. The results show that the multi-diameter NWA exhibits high and nearly flat absorption over a broad wavelength range due to the superposition of absorption peaks for NWs with different diameters. A remarkable efficiency of 17% is obtained for a 16-diameter NWA, higher than the best value (16.1%) of uniform-diameter device with an optimum diameter. The results suggest that the multi-diameter NWA solar cells have higher conversion efficiency than the uniform-diameter counterpart. Our work demonstrates that a practical self-organized NWA solar cell possesses higher efficiency than the ordered uniform-diameter NWA solar cell, with much lower cost and simpler fabrication process.

Funding

National Natural Science Foundation of China (61774021, 61504010, and 61674020), the Fundamental Research Funds for the Central Universities (2018XKJC05), the Fund of State Key Laboratory of Information Photonics and Optical Communications (Beijing University of Posts and Telecommunications), P. R. China (IPOC2017ZT02 and IPOC2017ZZ01), and the Hong Kong Scholars Program (XJ2018052).

References

1. H. Savin, P. Repo, G. von Gastrow, P. Ortega, E. Calle, M. Garín, and R. Alcubilla, "Black silicon solar cells with interdigitated back-contacts achieve 22.1% efficiency," Nat. Nanotechnol. **10**(7), 624–628 (2015).
2. H. A. Atwater and A. Polman, "Plasmonics for improved photovoltaic devices," Nat. Mater. **9**(3), 205–213 (2010).
3. J. G. Mutitu, S. Shi, C. Chen, T. Creazzo, A. Barnett, C. Honsberg, and D. W. Prather, "Thin film solar cell design based on photonic crystal and diffractive grating structures," Opt. Express **16**(19), 15238–15248 (2008).
4. M. Bernechea, N. C. Miller, G. Xercavins, D. So, A. Stavrinadis, and G. Konstantatos, "Solution-processed solar cells based on environmentally friendly $AgBiS_2$ nanocrystals," Nat. Photonics **10**(8), 521–525 (2016).
5. O. E. Semonin, J. M. Luther, S. Choi, H.-Y. Chen, J. Gao, A. J. Nozik, and M. C. Beard, "Peak external photocurrent quantum efficiency exceeding 100% via MEG in a quantum dot solar cell," Science **334**(6062), 1530–1533 (2011).

Optics EXPRESS

6. J. Wallentin, N. Anttu, D. Asoli, M. Huffman, I. Åberg, M. H. Magnusson, G. Siefer, P. Fuss-Kailuweit, F. Dimroth, B. Witzigmann, H. Q. Xu, L. Samuelson, K. Deppert, and M. T. Borgström, "InP nanowire array solar cells achieving 13.8% efficiency by exceeding the ray optics limit," Science **339**(6123), 1057–1060 (2013).
7. E. Garnett and P. Yang, "Light trapping in silicon nanowire solar cells," Nano Lett. **10**(3), 1082–1087 (2010).
8. P. Krogstrup, H. I. Jørgensen, M. Heiss, O. Demichel, J. V. Holm, M. Aagesen, J. Nygard, and A. Fontcuberta i Morral, "Single-nanowire solar cells beyond the Shockley–Queisser limit," Nat. Photonics **7**(4), 306–310 (2013).
9. M. T. Borgstrom, M. H. Magnusson, F. Dimroth, G. Siefer, O. Hohn, H. Riel, H. Schmid, S. Wirths, M. Bjork, I. Aberg, W. Peijnenburg, M. Vijver, M. Tchernycheva, V. Piazza, and L. Samuelson, "Towards nanowire tandem junction solar cells on silicon," IEEE J. Photovolt. **8**(3), 1 (2018).
10. M. Yao, S. Cong, S. Arab, N. Huang, M. L. Povinelli, S. B. Cronin, P. D. Dapkus, and C. Zhou, "Tandem solar cells using GaAs nanowires on Si: design, fabrication, and observation of voltage addition," Nano Lett. **15**(11), 7217–7224 (2015).
11. Z. Fan, H. Razavi, J. W. Do, A. Moriwaki, O. Ergen, Y. L. Chueh, P. W. Leu, J. C. Ho, T. Takahashi, L. A. Reichertz, S. Neale, K. Yu, M. Wu, J. W. Ager, and A. Javey, "Three-dimensional nanopillar-array photovoltaics on low-cost and flexible substrates," Nat. Mater. **8**(8), 648–653 (2009).
12. M. J. Bierman and S. Jin, "Potential applications of hierarchical branching nanowires in solar energy conversion," Energy Environ. Sci. **2**(10), 1050–1059 (2009).
13. J. Zhang, L. Ai, X. Yan, Y. Wu, W. Wei, M. Zhang, and X. Zhang, "Photovoltaic performance of pin junction nanocone array solar cells with enhanced effective optical absorption," Nanoscale Res. Lett. **13**(1), 306 (2018).
14. Y. Wu, X. Yan, X. Zhang, and X. Ren, "Enhanced photovoltaic performance of an inclined nanowire array solar cell," Opt. Express **23**(24), A1603–A1612 (2015).
15. X. Li, R. Zhang, N. Huang, T. Lü, and W. Cao, "Surface acoustic wave propagation properties in 0.67Pb(Mg(13)Nb(23))O(3)-0.33PbTiO(3) single crystal poled along [111](c)," Appl. Phys. Lett. **95**(24), 242906 (2009).
16. I. Åberg, G. Vescovi, D. Asoli, U. Naseem, J. P. Gilboy, C. Sundvall, A. Dahlgren, K. E. Svensson, N. Anttu, M. T. Björk, and L. Samuelson, "A GaAs nanowire array solar cell with 15.3% efficiency at 1 sun," IEEE J. Photovolt. **6**(1), 185–190 (2016).
17. M. Yao, N. Huang, S. Cong, C. Y. Chi, M. A. Seyedi, Y. T. Lin, Y. Cao, M. L. Povinelli, P. D. Dapkus, and C. Zhou, "GaAs nanowire array solar cells with axial p-i-n junctions," Nano Lett. **14**(6), 3293–3303 (2014).
18. G. Mariani, P.-S. Wong, A. M. Katzenmeyer, F. Léonard, J. Shapiro, and D. L. Huffaker, "Patterned radial GaAs nanopillar solar cells," Nano Lett. **11**(6), 2490–2494 (2011).
19. Z. Gu, P. Prete, N. Lovergine, and B. Nabet, "On optical properties of GaAs and GaAs/AlGaAs core-shell periodic nanowire arrays," J. Appl. Phys. **109**(6), 064314 (2011).
20. L. Wen, Z. Zhao, X. Li, Y. Shen, H. Guo, and Y. Wang, "Theoretical analysis and modeling of light trapping in high efficicency GaAs nanowire array solar cells," Appl. Phys. Lett. **99**(14), 143116 (2011).
21. J. Svensson, N. Anttu, N. Vainorius, B. M. Borg, and L. E. Wernersson, "Diameter-Dependent photocurrent in InAsSb nanowire infrared photodetectors," Nano Lett. **13**(4), 1380–1385 (2013).
22. D. Wu, X. Tang, K. Wang, and X. Li, "An analytic approach for optimal geometrical design of GaAs nanowires for maximal light harvesting in photovoltaic cells," Sci. Rep. **7**(1), 46504 (2017).
23. X. Ye, H. Huang, X. Ren, J. Guo, Y. Huang, Q. Wang, and X. Zhang, "Growths of InAs/GaAs and InAs/$In_xGa_{1-x}As$/GaAs nanowire heterostructures," Wuli Xuebao **60**(3), 036103 (2011).
24. J. Vukajlovic-Plestina, W. Kim, V. G. Dubrovski, G. Tütüncüoğlu, M. Lagier, H. Potts, M. Friedl, and A. Fontcuberta I Morral, "Engineering the Size Distributions of Ordered GaAs Nanowires on Silicon," Nano Lett. **17**(7), 4101–4108 (2017).
25. H. Y. Xu, Y. N. Guo, W. Sun, Z. M. Liao, T. Burgess, H. F. Lu, Q. Gao, H. H. Tan, C. Jagadish, and J. Zou, "Quantitative study of GaAs nanowires catalyzed by Au film of different thicknesses," Nanoscale Res. Lett. **7**(1), 589 (2012).
26. G. Mariani, Z. Zhou, A. Scofield, and D. L. Huffaker, "Direct-bandgap epitaxial core-multishell nanopillar photovoltaics featuring subwavelength optical concentrators," Nano Lett. **13**(4), 1632–1637 (2013).
27. M. Levinshtein, S. Rumyantsev, and M. Shur, *Handbook series on semiconductor parameters: ternary and quaternary III–V compounds* (World Scientific, 1996).
28. M. G. Deceglie, V. E. Ferry, A. P. Alivisatos, and H. A. Atwater, "Design of nanostructured solar cells using coupled optical and electrical modeling," Nano Lett. **12**(6), 2894–2900 (2012).
29. O. Demichel, M. Heiss, J. Bleuse, H. Mariette, and A. Fontcuberta i Morral, "Impact of surfaces on the optical properties of GaAs nanowires," Appl. Phys. Lett. **97**(20), 201907 (2010).
30. C. C. Chang, C. Y. Chi, M. Yao, N. Huang, C. C. Chen, J. Theiss, A. W. Bushmaker, S. Lalumondiere, T. W. Yeh, M. L. Povinelli, C. Zhou, P. D. Dapkus, and S. B. Cronin, "Electrical and optical characterization of surface passivation in GaAs nanowires," Nano Lett. **12**(9), 4484–4489 (2012).
31. N. Tajik, Z. Peng, P. Kuyanov, and R. R. LaPierre, "Sulfur passivation and contact methods for GaAs nanowire solar cells," Nanotechnology **22**(22), 225402 (2011).
32. H. Guo, L. Wen, X. Li, Z. Zhao, and Y. Wang, "Analysis of optical absorption in GaAs nanowire arrays," Nanoscale Res. Lett. **6**(1), 617 (2011).